THE JOURNAL OF BIOLOGICAL CHEMISTRY VOL. 287, NO. 17, pp. 14099–14108, April 20, 2012

Amino Acid Templating Mechanisms in Selection of Nucleotides Opposite Abasic Sites by a Family A DNA Polymerase*[S]

Received for publication, December 16, 2011, and in revised form, January 31, 2012 Published, JBC Papers in Press, February 8, 2012, DOI 10.1074/jbc.M111.334904

Samra Obeid[‡§1], **Wolfram Welte**[§¶], **Kay Diederichs**[§¶], **and Andreas Marx**[‡§2]

From the Departments of [‡]*Chemistry and* [¶]*Biology and the* [§]*Konstanz Research School Chemical Biology, University of Konstanz, Universitätsstrasse 10, D 78457 Konstanz, Germany*

Background: Abasic sites are the most frequent DNA lesions and are often bypassed by incorporating an adenosine opposite that lesion.
Results: We determined structures of DNA polymerase in complex with different nucleotides opposite an abasic site.
Conclusion: Interaction of the incoming nucleotide with a single amino acid governs nucleotide selection opposite abasic sites.
Significance: This work furthers the understanding of the bypass of a mutagenic lesion by DNA polymerases.

Cleavage of the *N*-glycosidic bond that connects the nucleobase to the backbone in DNA leads to abasic sites, the most frequent lesion under physiological conditions. Several DNA polymerases preferentially incorporate an A opposite this lesion, a phenomenon termed "A-rule." Accordingly, *KlenTaq*, the large fragment of *Thermus aquaticus* DNA polymerase I, incorporates a nucleotide opposite an abasic site with efficiencies of A > G > T > C. Here we provide structural insights into constraints of the active site during nucleotide selection opposite an abasic site. It appears that these confines govern the nucleotide selection mainly by interaction of the incoming nucleotide with Tyr-671. Depending on the nucleobase, the nucleotides are differently positioned opposite Tyr-671 resulting in different alignments of the functional groups that are required for bond formation. The distances between the α-phosphate and the 3′-primer terminus increases in the order A < G < T, which follows the order of incorporation efficiency. Additionally, a binary *KlenTaq* structure bound to DNA containing an abasic site indicates that binding of the nucleotide triggers a remarkable rearrangement of enzyme and DNA template. The ability to resolve the stacking arrangement might be dependent on the intrinsic properties of the respective nucleotide contributing to nucleotide selection. Furthermore, we studied the incorporation of a non-natural nucleotide opposite an abasic site. The nucleotide was often used in studying stacking effects in DNA polymerization. Here, no interaction with Tyr-761 as found for the natural nucleotides is observed, indicating a different reaction path for this non-natural nucleotide.

The most common DNA damage under physiological conditions consists of abasic sites resulting from spontaneous hydrolysis of the *N*-glycosidic bond between the sugar moiety and the nucleobase in DNA (1). Because the genetic information is lost by the cleavage of the nucleobase, abasic sites bear a high mutagenic potential (2–4). In most cases, the lesion is removed by DNA repair systems using the sister strand to guide for incorporation of the right nucleotide. However, undetected lesions, or those formed during S phase, pose a challenge to DNA polymerases and block replication (5, 6). Several studies indicated the mutagenic potential of these lesions in translesion synthesis, which is more pronounced in animal as compared with bacterial cells presumably due to higher translesion synthesis in eukaryotes (4, 7, 8). Interestingly, it has been shown that in human cells, an adenosine (A) is preferentially incorporated opposite abasic sites (4). Further *in vitro* and *in vivo* studies of DNA polymerases from family A (including human DNA polymerases γ and θ) and B (including human DNA polymerases α, ε, and δ) in the presence of the stabilized tetrahydrofuran abasic site analog F (supplemental Fig. S1) have shown that purines, in particular adenosine, and to a lesser extent guanosine, are most frequently incorporated opposite the lesion. The strong preference for adenosine has been termed "A-rule" (7–20).

A set of studies concerning the behavior of DNA polymerases from different sequence families showed that there are multiple mechanisms to overcome an abasic site. Most translesion DNA polymerases follow various loop-out mechanisms (11, 21–25). Thereby, the nucleotide selection is influenced by the following upstream templating bases resulting in deletions and complex mutation spectra. Recently, an amino acid templating mechanism was found for the "error-free" bypass of an abasic site by the yeast Rev1 DNA polymerase member of family Y (26). Because guanine is cleaved most frequently (2), the preference of Rev1 for dCMP incorporation opposite an abasic site represents the "best guess."

However, the determinants of the A-rule are still controversially discussed. Structural and functional studies have added significantly to our understanding of the basic mechanisms of

* This work was supported by the Deutsche Forschungsgemeinschaft through a grant in SPP 1170.
[S] This article contains supplemental Figs. S1–S7 and Table S1.
The atomic coordinates and structure factors (codes 3RR8, 3RRG, 3RRH, 3RR7, and 3T3F) have been deposited in the Protein Data Bank, Research Collaboratory for Structural Bioinformatics, Rutgers University, New Brunswick, NJ (http://www.rcsb.org/).
[1] Supported by funding from the Zukunftskolleg, University of Konstanz.
[2] To whom correspondence should be addressed: Dept. of Chemistry and Konstanz Research School Chemical Biology, University of Konstanz, Universitätsstrasse 10, D 78457 Konstanz, Germany. Tel.: 49-7531-885139; Fax: 49-7531-885140; E-mail: andreas.marx@uni-konstanz.de.

translesion synthesis by DNA polymerases (27, 28). Superior stacking as well as solvation properties of adenine have been discussed as the driving force behind adenine selection (17, 29–31). However, previously reported structures of *KlenTaq*, the large fragment of *Thermus aquaticus (Taq)* DNA polymerase I, which is a member of the sequence family A, suggests that this enzyme follows the A-rule by applying an amino acid templating mechanism (19, 20). Thereby, interaction with Tyr-671 seems to be the basis of the preference of purines. It facilitates nucleotide incorporation by mimicking a pyrimidine nucleobase directing for purine incorporation opposite abasic sites due to the enhanced geometric fit to the active site (32, 33). The crucial role of this tyrosine in translesion synthesis, which is highly conserved throughout evolution in DNA polymerase family A from bacteria to humans (34), was further probed by analysis of site-directed mutations (19). Interestingly, when the six-membered ring of tyrosine was mutated to the bicyclic indole of tryptophan, the A-rule was shifted to a "C/T-rule," further supporting geometric factors as determinants of nucleotide selection opposite an abasic site.

Still, several aspects remain to be clarified to fully understand the mechanism of nucleotide selection opposite an abasic site by DNA polymerases from the family A. These aspects include the overall conformation of the enzyme-DNA complex in the binary state prior to nucleotide binding. Furthermore, the order of nucleotide incorporation efficiency opposite abasic sites by DNA polymerases such as *KlenTaq* is A, G, T, and C. The mechanistic understanding for this observation is sparse due to the lack of structural data. Here, we report a structure of a binary complex of *KlenTaq* DNA polymerase bound to the primer/template bearing an abasic site lesion. Additionally, we present several ternary structures of *KlenTaq* caught incorporating different nucleotides opposite an abasic site, providing insights into the preference order of nucleotide incorporation efficiency opposite this lesion.

EXPERIMENTAL PROCEDURES

Protein and Oligonucleotides

Protein expression and purification were conducted as described (35). In brief, an *Escherichia coli* codon-optimized *KlenTaq* gene (amino acids 293–832 of *Taq* gene; purchased from GeneArt) was cloned into a pET-21b vector without any purification tags and expressed in *E. coli* strain BL21 (DE3). Of note, codon optimization resulted in changes within the gene sequence without affecting the amino acid sequence. After heat denaturation and ultracentrifugation, a PEI precipitation was performed. The resulting material was purified by anion exchange (Q Sepharose) chromatography followed by size-exclusion chromatography (Superdex 75) in 20 mM Tris HCl, pH 7.5, 150 mM NaCl, 1 mM EDTA, 1 mM β-mercaptoethanol.

Oligonucleotides were purchased from Metabion or Thermo Scientific. The dideoxy cytosine modified primer was synthesized on an Applied Biosystems 392 DNA/RNA synthesizer using 5′-dimethoxytrityl-2′,3′-dideoxy cytosine modified *N*-succinoyl-long chain alkylamino controlled pore glass, which was purchased from Glen Research. The synthesized oligonucleotide was purified by preparative PAGE on a 12% polyacrylamide gel containing 8 M urea (DMT-OFF). The nucleotide dNITP[3] was synthesized starting from dNI purchased from Berry & Associates Inc., according to published procedures (36).

Crystallization and Structure Determination

KlenTaq (buffer: 20 mM Tris HCl, pH 7.5, 150 mM NaCl, 1 mM EDTA, 1 mM β-mercaptoethanol) was incubated in the presence of DNA primer (5′-d(GAC CAC GGC GC)-3′), an abasic site F containing template (5′-d(AAA FNG CGC CGT GGT C)-3′); N represents the templating base directing the processing of ddGTP, ddTTP, or ddCTP.

KlenTaq$_{F\text{-}G\text{-}I}$—The crystallization was set up using purified *KlenTaq* (11 mg/ml), DNA template/primer duplex, and ddGTP in a molar ratio of 1:3:50 and in the presence of 20 mM $MgCl_2$. The crystallization solution was mixed in a 1:1 ratio with the reservoir solution containing 0.05 M sodium cacodylate (pH 6.5), 0.2 M NH_4OAc, 0.01 M $Mg(OAc)_2$, and 25% PEG 8000.

KlenTaq$_{F\text{-}G\text{-}II}$—The crystallization was set up as for *KlenTaq*$_{F\text{-}G\text{-}I}$ except using *KlenTaq* (11 mg/ml):DNA template/primer duplex:ddGTP = 1:3:50 in the presence of 20 mM $MgCl_2$. The reservoir solution contained 0.05 M sodium cacodylate (pH 6.5), 0.2 M NH_4OAc, 0.01 M $Mg(OAc)_2$, and 28% PEG 8000.

KlenTaq$_{F\text{-}T}$—The crystallization was set up as for *KlenTaq*$_{F\text{-}G\text{-}I}$ except using *KlenTaq* (11 mg/ml):DNA template/primer duplex:ddTTP = 1:3:50 in the presence of 20 mM $MgCl_2$. The reservoir solution contained 0.05 M sodium cacodylate (pH 6.5), 0.2 M NH_4OAc, 0.01 M $Mg(OAc)_2$, and 28% PEG 8000.

KlenTaq$_{F\text{-}binary\text{-}II}$—The crystallization was set up as for *KlenTaq*$_{F\text{-}G\text{-}I}$ except using *KlenTaq* (11 mg/ml):DNA template/primer duplex:ddCTP = 1:1.5:60 in the presence of 20 mM $MgCl_2$. The reservoir solution contained 0.1 M Tris HCl (pH 8.0), 0.2 M $Mg(formiate)_2$, and 15% PEG 8000.

KlenTaq$_{F\text{-}binary}$—The crystallization was set up using purified *KlenTaq* (8 mg/ml), a template (5′-d(AAA FGG CGC CGT GGT C)-3′), and a previously synthesized primer with a dideoxy cytosine at its 3′-end, in a molar ratio of 1:1.4 and in the presence of 20 mM $MgCl_2$. The crystallization solution was mixed in 1:1 ratio with the reservoir solution containing 0.1 M Tris HCl (pH 7.5), 0.2 M $Mg(formiate)_2$, and 12% PEG 8000.

KlenTaq$_{F\text{-}NI}$—The crystallization was set up as for *KlenTaq*$_{F\text{-}binary}$ except using *KlenTaq* (8 mg/ml):DNA template/primer duplex = 1:1.4 and in the presence of 20 mM $MgCl_2$. The reservoir solution contained 0.1 M Tris HCl (pH 7.0), 0.2 M $Mg(formiate)_2$, and 18% PEG 8000. The crystals were soaked overnight by adding 0.5 μl of dNITP (20 mM) solution. The occupancy of the bound dNITP was refined to 0.77.

Crystals were produced by the hanging drop vapor diffusion method by equilibrating against 1 ml of the reservoir solution for 5 days at 18 °C. The crystals were frozen in liquid nitrogen.

[3] The abbreviations used are: dNITP, 5-nitroindolyl-2′-deoxyriboside 5′-triphosphate; ddTTP, dideoxythymidine 5′-triphosphate; r.m.s.d., root mean square deviation; dNIMP, 5-nitroindoyl-2′-deoxyriboside 5′-monophosphate; ddGTP, dideoxyguanosine 5′-triphosphate; ddCTP, dideoxycytidine 5′-triphosphate; ddATP, dideoxyadenosine 5′-triphosphate; ddNTP, dideoxynucleoside 5′-triphosphate.

Datasets were collected at beamline PXI (X06SA) of the Swiss Light Source (Paul Scherrer Institute, Villigen, Switzerland), at a wavelength of 1.000 or 0.900 Å using a PILATUS 6M detector. Data reduction was performed with the XDS package (37, 38). The structures were solved by difference Fourier techniques using *KlenTaq* wild type (Protein Data Bank (PDB) 3LWL) as model. Refinement was performed with PHENIX (39), and model rebuilding was done with COOT (40). Figures were made with PyMOL (41).

Primer Extension Assays

Primer extension was performed as described (19). In brief, for incorporation opposite F, 20 μl of the *KlenTaq* reactions contained 100 nM primer (5′-d(CGT TGG TCC TGA AGG AGG ATA GG)-3′), 130 nM template (5′-d(AAA TCA FCC TAT CCT CCT TCA GGA CCA ACG TAC)-3′), 100 μM dNTPs in buffer (20 mM Tris HCl, pH 7.5, 50 mM NaCl, and 2 mM $MgCl_2$), and 500 nM of the respective *KlenTaq* polymerase. Reaction mixtures were incubated at 37 °C. Incubation times are provided in the respective figure legends. Primer was labeled using [γ-^{32}P]ATP according to standard techniques. Reactions were stopped by the addition of 45 μl of stop solution (80% (v/v) formamide, 20 mM EDTA, 0.25% (w/v) bromphenol blue, 0.25% (w/v) xylene cyanol) and analyzed by 12% denaturing PAGE. Visualization was performed by phosphorimaging.

Enzyme Kinetics

The rates of single turnovers in pre-steady-state kinetics were determined as described (19). In brief, 15 μl of radiolabeled primer/template complex (200 nM) and DNA polymerase (2 mM) in reaction buffer (see primer extension assay) were rapidly mixed with 15 μl of a dNTP solution in reaction buffer at 37 °C. Quenching was achieved by adding previously described stop solution. For reaction times longer than 5 s, a manual quench was performed. The analysis of dNTP incorporation opposite to the abasic site primer (for sequences, see "Primer Extension Assays") and templates (for sequences, see "Primer Extension Assays") were applied. Quenched samples were analyzed on a 12% denaturing PAGE followed by phosphorimaging. For kinetic analysis, experimental data were fit by nonlinear regression using the program GraphPad Prism 4. The data were fit to a single exponential equation: (conversion) = $A \times (1 - \exp(-k_{obs}\, t))$. The observed catalytic rates (k_{obs}) were then plotted against the dNTP concentrations used, and the data were fit to a hyperbolic equation to determine the K_d of the incoming nucleotide. The incorporation efficiency is given by k_{pol}/K_d.

RESULTS

Overall Structure of KlenTaq Complexes in Presence of an Abasic Site—All *KlenTaq* crystals grew in the same space group and very similar cell parameters (supplemental Table S1) as those reported earlier (19, 20, 35, 42–45). Thus, significant differences in crystal packing forces acting on the active site should be negligible. Nevertheless, parts of the finger domain differ in their mobility (as measured by temperature factors) between the different structures. This is a consequence of the structural differences, which were induced in the active site assembly by the primer/template complexes and respective nucleotides that were investigated. In the following, the active sites for the various complexes are shown and described in detail.

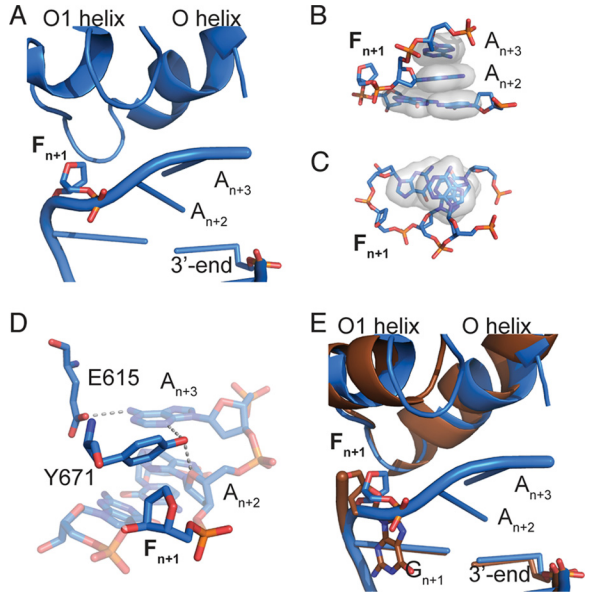

FIGURE 1. **Structure of *KlenTaq*$_{F\text{-}binary}$ (*blue*).** *A*, template stacking assembly of A_{n+2} and A_{n+3} in *KlenTaq*$_{F\text{-}binary}$. The abasic site analog F_{n+1} is located extrahelically. *B*, the stick and surface depiction highlights the template stacking arrangement. *C*, top view of the primer/template stacking arrangement. *D*, hydrogen-bonding network of the amino acid side chains Tyr-671 and Glu-615 with the template strand. *E*, same arrangement as in *A* for the superimposed structures of *KlenTaq*$_{F\text{-}binary}$ (*blue*) and *KlenTaq*$_{binary}$ (*brown*).

Structure of KlenTaq in Binary Complex with DNA Duplex Containing an Abasic Site (KlenTaq$_{F\text{-}binary}$*)*—To address the issue, if the overall conformation of the enzyme-DNA complex is affected by an abasic site prior to nucleotide binding, we crystallized *KlenTaq* bound to primer/template duplex containing an abasic site following a similar strategy as reported recently (19, 20, 35, 43, 46). The structure was solved by difference Fourier techniques at a resolution of 1.9 Å (supplemental Table S1). *KlenTaq*$_{F\text{-}binary}$ is very similar to one reported for *KlenTaq* in a binary complex bound to undamaged DNA duplex (PDB 4KTQ; *KlenTaq*$_{binary}$) (35) as reflected by an r.m.s.d. for C_α atoms of 0.60 Å (Fig. 1). However, remarkable structural changes were observed for the single-stranded 5′-overhang of the DNA template, which is rotated around the helical axis. Thereby, the lesion is flipped out of a developing DNA duplex (Fig. 1*A*). This conformation is stabilized by stacking of the 5′-upstream nucleobases of the template strand on the top of the primer/template duplex (Fig. 1, *B* and *C*) and a distinct hydrogen-bonding network of amino acid residues Glu-615 and Tyr-671 with the DNA template (Fig. 1*D*). In contrast, in *KlenTaq*$_{binary}$, the backbone rotates 5′ to the DNA duplex, redirecting the remainder of the single-stranded template out of the DNA polymerase active site (Fig. 1*E*).

KlenTaq with ddGTP Opposite an Abasic Site (KlenTaq$_{F\text{-}G\text{-}I}$ *KlenTaq*$_{F\text{-}G\text{-}II}$*)*—To gain insights into the structural basis for the preference of adenosine over guanosine of *KlenTaq* in bypassing an abasic site, we crystallized *KlenTaq* as a ternary complex bound to a primer/template duplex and ddGTP oppo-

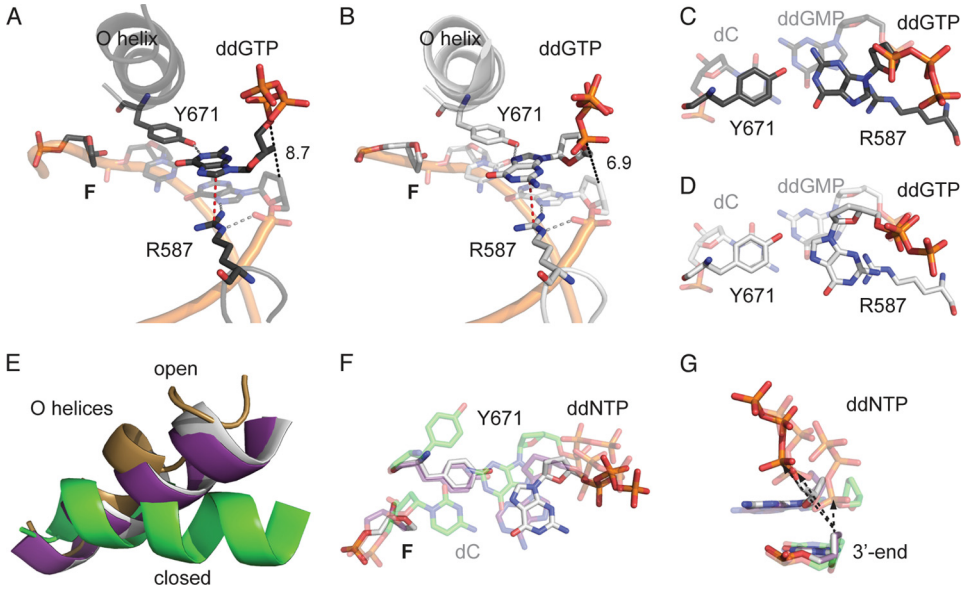

FIGURE 2. **Structure of *KlenTaq*$_{F\text{-}G\text{-}I}$ (*black*) and *KlenTaq*$_{F\text{-}G\text{-}II}$ (*gray*).** *A*, stabilization network of ddGTP in *KlenTaq*$_{F\text{-}G\text{-}I}$. The amino acid side chains Arg-587 and Tyr-671 are labeled. *Gray*, *red*, and *black dashed lines* indicate hydrogen-bonding interactions, cation-π interaction, and distance (Å), respectively. *B*, the same as in *A* for *KlenTaq*$_{F\text{-}G\text{-}II}$. *C*, top view of the nascent base pair opposite F (*KlenTaq*$_{F\text{-}G\text{-}I}$). In the front, the incoming ddGTP opposite Tyr-671 is depicted. The first nucleobase pair of the primer/template terminus is shown as transparent. *D*, same view as in *C* for *KlenTaq*$_{F\text{-}G\text{-}II}$. *E*, the O helices from the superimposition of *KlenTaq*$_{F\text{-}G\text{-}II}$ (*gray*), *KlenTaq*$_{F\text{-}A}$ (*purple*), *KlenTaq*$_{C\text{-}G}$ (*green*), and *KlenTaq*$_{open}$ (*gold*) are highlighted. *F*, comparison of the nascent base pairs of *KlenTaq*$_{F\text{-}G\text{-}II}$ (*gray*), *KlenTaq*$_{F\text{-}A}$ (*purple*), and *KlenTaq*$_{C\text{-}G}$ (*green*). *G*, the incoming ddNTPs of *KlenTaq*$_{F\text{-}G\text{-}II}$ (*gray*), *KlenTaq*$_{F\text{-}A}$ (*purple*), and *KlenTaq*$_{C\text{-}G}$ (*green*) and the respective 3′-primer terminus are shown. The *arrow* indicates the displacement of the α-phosphate regarding to the 3′-primer terminus.

site the abasic site. Two structures were reproducibly found in several crystallization trials and solved by difference Fourier techniques at resolutions of 2.3–2.4 Å (*KlenTaq*$_{F\text{-}G\text{-}I}$ and *KlenTaq*$_{F\text{-}G\text{-}II}$) (supplemental Table S1). The obtained structures show conformational heterogeneity in the active site region. In particular, we found two different orientations of the incoming ddGTP (Fig. 2, *A* and *B*, and supplemental Fig. S2, *A* and *B*). However, the overall conformation of the two ddGTP-trapped structures is very similar to the ternary complex of *KlenTaq* harboring ddATP opposite an abasic site (PDB 3LWL; *KlenTaq*$_{F\text{-}A}$; r.m.s.d. for Cα of 0.42 Å) (19), showing the same remarkable structural changes as compared with the undamaged case (*KlenTaq* bound to an undamaged primer/template duplex processing a ddGTP; PDB 1QSS; *KlenTaq*$_{C\text{-}G}$) (42). Thus, the conformation of the O helix leaves the active site more open, similar to the one in *KlenTaq*$_{F\text{-}A}$, and somehow between the open (PDB 2KTQ; *KlenTaq*$_{open}$) (35) and closed (*KlenTaq*$_{C\text{-}G}$) conformations in the reported ternary complexes (Fig. 2*E*). Like in *KlenTaq*$_{F\text{-}A}$, we found that the abasic site is intrahelically located and that Tyr-671 is positioned opposite the incoming ddGTP at the place that is usually occupied by the templating nucleobase (Fig. 2*A*). However, remarkable differences between *KlenTaq*$_{F\text{-}A}$ and *KlenTaq*$_{F\text{-}G\text{-}I}$ appear in the positioning and interaction pattern of the incoming triphosphates (Fig. 2*A* and supplemental Fig. S3, *A* and *B*). In *KlenTaq*$_{F\text{-}G\text{-}I}$, Tyr-671 stabilizes ddGTP via hydrogen bonds between the Tyr-671 hydroxyl group and the N1 of guanine, whereas in *KlenTaq*$_{F\text{-}A}$, the N3 of adenine interacts with Tyr-671 (Fig. 2*A* and supplemental Fig. S3*A*). Furthermore, an important stabilizing factor of the incoming nucleotide is Arg-587. In *KlenTaq*$_{F\text{-}A}$, Arg-587 forms a hydrogen bond to the N7 of adenine (supplemental Fig. S3*A*). However, in *KlenTaq*$_{F\text{-}G\text{-}I}$, ddGTP is stabilized by cation-π interaction with Arg-587. Because this type of interaction strongly depends on the distribution of the electron density in the aromatic ring system, there is in the case of purines a clear preference for arginine to position itself below or above the imidazole five-atom ring system (47). Indeed, this is observed in *KlenTaq*$_{F\text{-}G\text{-}I}$ for Arg-587 (Fig. 2, *A* and *C*). The binding arrangement of ddGTP causes a misalignment of the α-phosphate, resulting in a large distance of the α-phosphate to the 3′-primer terminus (8.7 Å). Hence, *KlenTaq*$_{F\text{-}G\text{-}I}$ might represent an initial binding event of the incoming triphosphate (Fig. 2*A*). In comparison, the guanine base in *KlenTaq*$_{F\text{-}G\text{-}II}$ is rotated around the *N*-glycosidic bond, and the N7 of guanine points to the hydroxyl group of Tyr-671 (Fig. 2, *B* and *D*, and supplemental Fig. S2*B*). Thereby, the sugar moiety is realigned, resulting in a shortened distance between the α-phosphate and 3′-primer terminus of about 6.9 Å. However, the reorientation of the nucleobase positions the six-membered heterocycle above Arg-587 (Fig. 2, *B* and *D*), a less favored arrangement observed only in rare cases (47). In summary, the distance between 3′-OH and the α-phosphate increases in the following direction *KlenTaq*$_{F\text{-}A}$ < *KlenTaq*$_{F\text{-}G\text{-}II}$ < *KlenTaq*$_{F\text{-}G\text{-}I}$ that are all longer than the one observed in the canonical case (Fig. 2*G*).

Pyrimidines Opposite an Abasic Site—Pyrimidine nucleotides are incorporated opposite an abasic site by *KlenTaq* with poor efficiencies (19). Furthermore, we demonstrated that the purine preference could be switched to pyrimidine preference by a single site-directed mutagenesis of Tyr-671 to Trp (19). This suggests that the low incorporation efficiencies of pyrimidines relies on a specific interaction with this amino acid residue. To get structural insights, we crystallized *KlenTaq* in the presence of a primer/template duplex and ddTTP. The structure was solved by difference Fourier techniques at a resolution

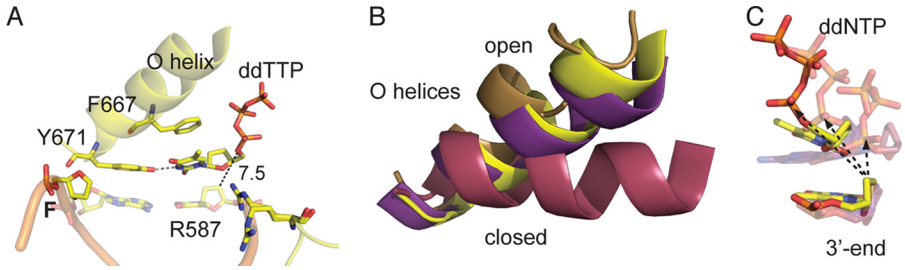

FIGURE 3. **Structure of *KlenTaq*$_{F\text{-}T}$ (*yellow*).** *A*, stabilization network of ddTTP. The amino acid side chains Arg-587, Phe-667, and Tyr-671 are labeled. *Gray* and *black dashed lines* indicate hydrogen-bonding interactions and distance (Å), respectively. *B*, the O helices from the superimposition of *KlenTaq*$_{F\text{-}T}$ (*yellow*), *KlenTaq*$_{F\text{-}A}$ (*purple*), *KlenTaq*$_{A\text{-}T}$ (*magenta*), and *KlenTaq*$_{binary}$ (*gold*) are highlighted. *C*, the incoming ddNTPs of *KlenTaq*$_{F\text{-}T}$ (*yellow*), *KlenTaq*$_{F\text{-}A}$ (*purple*), and *KlenTaq*$_{A\text{-}T}$ (*berry*) and the respective 3′-primer terminus are shown. The *arrow* indicates the displacement of the α-phosphate regarding the 3′-primer terminus.

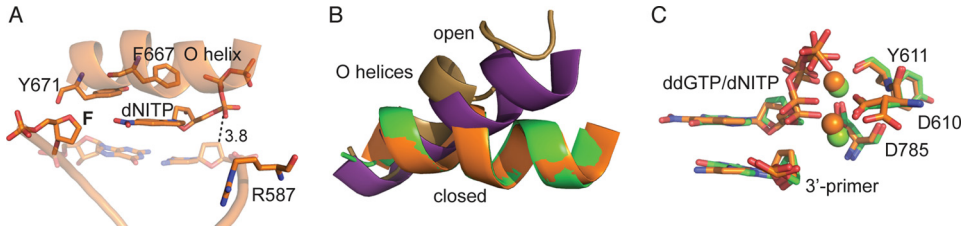

FIGURE 4. **Structure of *KlenTaq*$_{F\text{-}NI}$ (*orange*).** *A*, stabilization network of dNITP. The amino acid side chains Arg-587, Phe-667, and Tyr-671 are labeled. *Black dashed lines* indicate distance (Å). *B*, the O helices from the superimposition of *KlenTaq*$_{F\text{-}NI}$ (*cyan*), *KlenTaq*$_{F\text{-}A}$ (*purple*), *KlenTaq*$_{C\text{-}G}$ (*green*), and *KlenTaq*$_{binary}$ (*gold*) are highlighted. *C*, the incoming ddNTPs of *KlenTaq*$_{F\text{-}NI}$ (*cyan*) and *KlenTaq*$_{C\text{-}G}$ (*green*), the respective Mg^{2+} ions, and the respective catalytically relevant residues Asp-610, Tyr-611, and Asp-785 are shown.

of 1.8 Å (*KlenTaq*$_{F\text{-}T}$) (supplemental Table S1). Although kinetic studies elucidated that thymidine incorporation opposite an abasic site is unfavorable, we observed a bound thymidine triphosphate in the active site (Fig. 3*A* and supplemental Fig. S2*C*). Once more we obtained a semiclosed enzyme conformation as can be seen from the superimposition of this structure with *KlenTaq*$_{A\text{-}T}$ (PDB 1QTM; processing a canonical base pair with an incoming ddTTP) (42), *KlenTaq*$_{F\text{-}A}$, and *KlenTaq*$_{open}$ (Fig. 3*B*). The O helix does not pack against the nascent base pair, allowing Tyr-671 to position itself between the incoming ddTTP and the abasic site as is observed for Tyr-671 in *KlenTaq*$_{F\text{-}A}$ (Fig. 3*A* and supplemental Fig. S3*A*). The ddTTP is stabilized via H-bonding between the N1 of thymidine and the hydroxyl group of Tyr-671 as well as π-stacking interactions to Phe-667. In contrast to *KlenTaq*$_{F\text{-}A}$ in *KlenTaq*$_{F\text{-}T}$, Arg-587 is released from the stabilization pattern of the incoming triphosphate, as observed for the purine-trapped structures, while still interacting with the phosphate backbone of the 3′-primer terminus. The resulting thymidine tyrosine pair is accommodated in the active site in a way that results in a misalignment of the α-phosphate and thereby positions the sugar moiety on top of the 3′-primer terminus (Fig. 3*C*).

The same approach as described before was used to co-crystallize *KlenTaq* in the presence of a primer/template duplex and ddCTP (*KlenTaq*$_{F\text{-}binary\text{-}II}$). However, in all conducted approaches, only the formations of binary complexes of *KlenTaq* and the primer/template were obtained. These structures are very similar to the binary structure *KlenTaq*$_{F\text{-}binary}$ (supplemental Fig. S4).

Nucleotide Analog dNITP Incorporation Opposite an Abasic Site—Base stacking capability was suggested to play a decisive role in influencing the incorporation efficiency opposite an abasic site (17, 31, 48–50). Intriguingly, nucleotides that bear nucleobase surrogates with strong stacking but lacking hydrogen-bonding capability such as dNITP (Fig. 5*A*) are incorporated opposite abasic sites with higher efficiency as their natural counterparts. Therefore, non-natural nucleotides such as dNITP were used to investigate abasic site bypass as a probe for stacking. To get insights into how dNITP is processed opposite an abasic site by *KlenTaq*, we performed soaking experiments with crystals of a binary complex of *KlenTaq* in the presence of an abasic site and dNITP. The structure was solved by difference Fourier techniques at a resolution of 1.9 Å (supplemental Table S1 and supplemental Fig. S2*D*). In the presence of dNITP, the enzyme is accumulated in a closed and productive complex, very similar to reported canonical cases (*e.g.* PDB 1QTM; *KlenTaq*$_{A\text{-}T}$; r.m.s.d. for Cα of 0.53 Å) and in contrast to *KlenTaq*$_{F\text{-}A}$ (Fig. 4, *A* and *B*). In disparity with the structures of *KlenTaq* complexed with natural nucleotides opposite an abasic site, Tyr-671 is released from its stacking interaction to the template strand and provides space for the incoming dNITP (Fig. 4*A*). The hydrophobic nucleotide analog perfectly stacks on the developing DNA duplex, resulting in a proper alignment of the α-phosphate and recruitment of two catalytically essential magnesium ions (Fig. 4*C* and supplemental Fig. S5).

Furthermore, kinetics show that dNIMP is incorporated more efficiently than any other natural nucleotide by *KlenTaq* opposite an abasic site resulting in the following order of incorporation efficiencies (k_{pol}/K_d): NI $\gg$ A > G $\gg$ T > C (Fig. 5*C* and supplemental Fig. S6*A*). Due to the decrease in K_d and simultaneous increase in k_{pol}, dNIMP shows a 22-fold increase in incorporation efficiency as compared with dAMP. Interestingly, if *KlenTaq* mutant Y671W is used, we obtained the following incorporation efficiency (k_{pol}/K_d) order: NI > C > T $\gg$ A > G (Fig. 5*D* and supplemental Fig. S6*B*). Therefore, one can assume that Tyr-671 does not influence the incorporation of

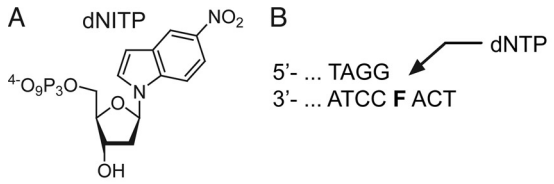

C

KTQ wt

N: -	NI	A	G	T	C
time:					
24 nt					
23 nt					

N/F-dNTP	K_d [μM]	k_{pol} [s^{-1} x10^{-2}]	k_{pol}/K_d [$M^{-1}*s^{-1}$ x10^{-4}]
T-dATP*	15.3±4.7	516±44	3373
F-dATP*	149±35	2.73±0.23	1.83
F-dNITP	19.7±1.1	7.80±1.12	39.5

D

KTQ Y671W

N: -	NI	A	G	T	C
time:					
24 nt					
23 nt					

N/F-dNTP	K_d [μM]	k_{pol} [s^{-1} x10^{-2}]	k_{pol}/K_d [$M^{-1}*s^{-1}$ x10^{-4}]
T-dATP*	363±104	91.6±15.2	25.2
F-dCTP*	845±161	0.92±0.12	0.11
F-dATP*	514±182	0.10±0.02	0.02
F-dNITP	97.8±24.4	0.24±0.02	0.25

FIGURE 5. **Nucleotide incorporation opposite an abasic site analog F.** *A*, structure of nucleotide analog dNITP. *B*, partial primer/template sequence used in primer extension experiments. *C*, single nucleotide (*nt*) incorporation of *KlenTaq* wild type opposite F for 1, 10, or 60 min, respectively. The respective dNTP is indicated. Transient kinetic analysis of nucleotide incorporation opposite T/F by *KlenTaq* wild type was performed. *, kinetic data were first reported in Ref. 19. *D*, single nucleotide incorporation of *KlenTaq* Y671W mutant opposite F for 10, 60, or 120 min, respectively. The respective dNTP is indicated. Transient kinetic analysis was performed as in *C* for *KlenTaq* Y671W.

dNIMP, whereas it clearly directs the incorporation of the natural nucleotides.

DISCUSSION

General Aspects—Although the bypass of a non-instructive lesion by DNA polymerases is extensively studied, the mechanisms are not fully understood yet. Besides initial binding of the nucleotide and the chemical reaction, noncovalent intermediates with energetic minima are crucial for the reaction pathway. These intermediates are believed to be responsible for preselection of nucleotides and represent kinetic checkpoints explaining the overall accuracy and fidelity of these enzymes (51–53). The present structural study provides further insights into how *KlenTaq* DNA polymerase, a member of sequence family A DNA polymerases, is able to bypass abasic sites (Table 1). Independent of the incoming natural nucleotide opposite the abasic site, the obtained ternary complexes show two noticeable alterations as compared with the canonical cases. Firstly, it is always observed that Tyr-671 is placed opposite the incoming nucleotides, and secondly, the enzyme adopts a semiclosed conformation. Such a conformation was also associated with mismatch incorporation (54). However, FRET studies of Klenow fragment DNA polymerase in the presence of mismatches indicate that along with the open form, the closed state is also partially occupied (55). Because crystallographic data only provide single snapshots, it is likely that in solution, there is also a distribution of the populations between the open and closed state even in the presence of an abasic site. Similarly to nucleotide discrimination between matched and mismatched nucleotides, DNA polymerases might also undergo several conformational changes as preselection steps before preceding the phosphoryl transfer in the presence of an abasic site. Therefore, the observed conformations might represent various local energy minima along the reaction coordinate. Along these lines, computer simulations of the fidelity of T7 DNA polymerase support the hypothesis that the formation of mismatches may also occur with high energy barriers from a partially open protein conformation (56). In general, there is an ongoing discussion whether the chemical step demands similar conformational states processing a correct or incorrect nucleotide (52–54, 57). However, the incoming nucleotides opposite an abasic site in the herein depicted structures are not properly aligned for the phosphoryl transfer. This suggests either that a rearrangement to the closed conformation has to occur or that the incorporation step proceeds from the semiclosed conformation after appropriate conformational changes of the nucleotide. Both scenarios support the observed overall poor incorporation efficiencies opposite abasic sites (19).

Structure of Binary Complex Containing Abasic Site and KlenTaq—In the binary complex of *KlenTaq* bound to an abasic site, we observed the 5′-upstream template strand stacking on the primer/template duplex. Nucleotide binding forces the release of the template strand from its stacking arrangement and triggers a remarkable rearrangement of the bound DNA template rather than a reorganization of the enzyme (supplemental Fig. S7). Furthermore, the ability to resolve the stacking arrangement might be dependent on the intrinsic properties of the respective nucleotide, such as the stacking and solvation ability of the nucleobase. It remains to be elucidated whether this arrangement is sequence-specific.

Nucleotide Selection Opposite Abasic Sites of KlenTaq, Adenosines versus Guanosines—The structural data offer valuable clues how nucleotide selection is performed opposite a non-instructive lesion and moreover support the previous kinetic analysis of abasic site bypass by *KlenTaq* (19). In the case of an incoming guanosine, we obtained several crystal structures showing the incoming triphosphate in two different orientations. This heterogeneity was not observed in the presence of the other nucleotides. In $KlenTaq_{F\text{-}G\text{-}I}$ and $KlenTaq_{F\text{-}G\text{-}II}$, Tyr-671 is filling the space of the vacant nucleobase of the abasic site and is located opposite the incoming ddGTP and thereby roughly mimics the geometry of a nascent nucleobase pair. Of note, such a selection of purines mediated by Tyr-671 is also observed for $KlenTaq_{F\text{-}A}$. However, in $KlenTaq_{F\text{-}G\text{-}I}$ and $KlenTaq_{F\text{-}G\text{-}II}$, the interaction with Tyr-671 causes misalignment of the α-phosphate resulting in enlarged distances to the 3′-primer terminus (Figs. 2*F* and 6, *A* and *B*). The different steric constraints of the purine structures account for the preference of adenosine over guanosine. In detail, the exocyclic

TABLE 1
Summary of *KlenTaq* structures bound to an abasic site analog F

F - A	F - G-I	F - G-II	F - T	F - binary	F - NI
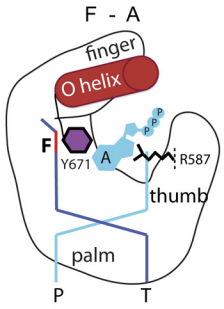	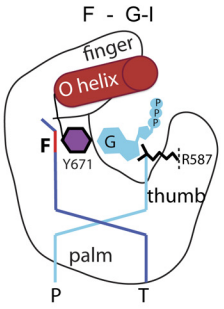	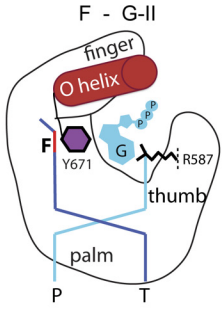	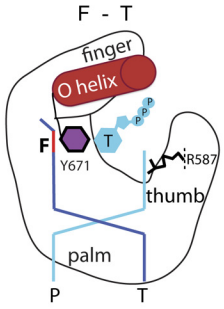	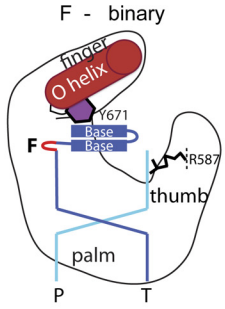	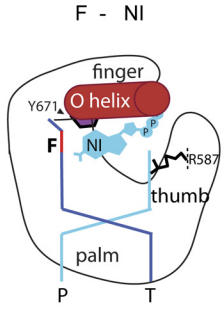
Y671 positioned opposite ddATP	Y671 positioned opposite ddGTP	Y671 positioned opposite ddGTP	Y671 positioned opposite ddTTP	Y671 is released from stacking interaction to the template strand	Y671 is released from stacking interaction to the template strand
H-bond N3-ddATP – OH-Y671	H-bond N1-ddGTP – OH-Y671	H-bond N7-ddGTP – OH-Y671	H-bond N1-ddTTP – OH-Y671	--	--
R587 stabilizes the phosphate-backbone of the 3'-primer terminus	R587 stabilizes the phosphate-backbone of the 3'-primer terminus	R587 stabilizes the phosphate-backbone of the 3'-primer terminus	R587 stabilizes the phosphate-backbone of the 3'-primer terminus	R587 stabilizes the phosphate-backbone of the 3'-primer terminus	R587 stabilizes the phosphate-backbone of the 3'-primer terminus
H-bond N7-ddATP – R587	cation-π interaction between 5-cyclic ring and R587	cation-π interaction between 6-cyclic ring and R587	--	--	--
F located intrahelically	F located intrahelically	F located intrahelically	F located intrahelically	F located extrahelically	F located intrahelically
1 Mg^{2+} ion is complexed by ddATP	--	--	1 Mg^{2+} ion is complexed by ddTTP	--	2 Mg^{2+} ion are complexed by ddNITP
P_α – 3'-primer terminus: 5.9 Å	α-P – 3'-primer terminus: 8.7 Å	α-P – 3'-primer terminus: 6.9 Å	α-P – 3'-primer terminus: 7.5 Å	--	α-P – 3'-primer terminus: 3.8 Å
PDB-ID: 3LWL	PDB-ID: 3RR8	PDB-ID: 3RRG	PDB-ID: 3RRH	PDB-ID: 3RR7	PDB-ID: 3T3F

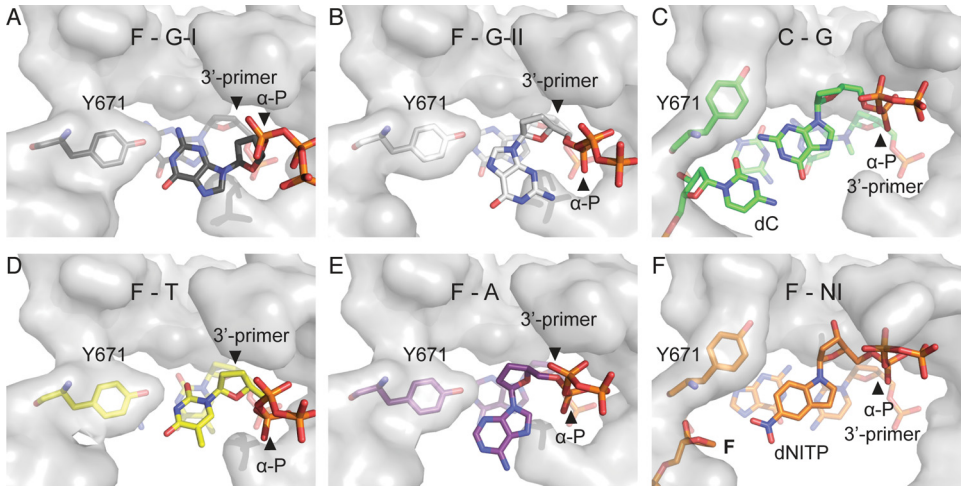

FIGURE 6. **Geometry fit to active site.** *A*, active site assembly in the presence of an abasic site analog F. The nascent base pair of Tyr-671 and ddGTP (*KlenTaq*$_{F\text{-}G\text{-}I}$) is depicted. The surface of the surrounding active site residues is shown in *gray*. *B*, same as in *A* for *KlenTaq*$_{F\text{-}G\text{-}II}$. *C*, active site assembly in the case of an undamaged template showing the nascent base pair of dC and ddGTP (*KlenTaq*$_{C\text{-}G}$). *D*, same as in *A* for *KlenTaq*$_{F\text{-}T}$. *E*, same as in *A* for *KlenTaq*$_{F\text{-}A}$. *F*, same as in *C* for *KlenTaq*$_{F\text{-}NI}$ showing the nascent base pair of F and dNITP. *A–F*, the arrows indicate the positioning of the α-phosphate and the 3′-primer terminus, respectively.

C_2-NH_2 group of guanine prevents the same arrangement of the nucleotide, as was found for adenosine (Table 1). Due to the steric restriction of the active site, the assembly of the sterically more demanding guanosine results in an alignment with an enlarged distance between the α-phosphate and the 3′-primer terminus in comparison with adenosine. Interestingly, the complex showing the stronger cation-π interaction between the Arg-587 and the five-membered ring (*KlenTaq*$_{F\text{-}G\text{-}I}$) results in an arrangement of the ddGTP obviating a possible attack at the α-phosphate. The closer orientation of the nucleotide toward the 3′-primer terminus suggests that the structure of *KlenTaq*$_{F\text{-}G\text{-}II}$ forming a less stable cation-π interaction (47) may represent one step ahead on the reaction coordinate in comparison with *KlenTaq*$_{F\text{-}G\text{-}I}$. In conclusion, we find that the distance between the α-phosphates and the 3′-primer terminus (see Table 1, 8.7–6.9 Å for guanosines *versus* 5.9 Å for adeno-

sine) correlates well with the measured incorporation efficiencies. This indicates that active misalignment of the incoming guanosines governs their unfavorable processing by *KlenTaq* in comparison with adenosines.

Nucleotide Selection Opposite Abasic Sites by KlenTaq, Purines versus Pyrimidines—To shine light on the incorporation mechanisms of the less favored pyrimidines, we investigated a structure bearing an incoming ddTTP opposite an abasic site. The DNA polymerase interacts with the incoming nucleotide by hydrogen bonding of Tyr-671 with the nucleobase. This results in a nucleoside triphosphate conformation where the sugar moiety is positioned above the 3′-primer terminus instead of the α-phosphate (Figs. 3*C* and 6*D*). In this scenario, all components of the active site are assembled and organized in a topological and geometrical arrangement that does not allow the enzyme to proceed with the chemical step, explaining the very low incorporation efficiency. In contrast to purines, ddTTP shows low *B*-factors (supplemental Table S1), which indicates that it is well stabilized opposite Tyr-671. Thus, the tightly bound thymidine probably stalls the DNA polymerase in a "nonproductive" complex by active misalignment, whereas the purine nucleobases enhance the geometric fit to the active site, resulting in an arrangement with shortened distances between the α-phosphate and the 3′-primer terminus as compared with the pyrimidine base (Figs. 2*G* and 6, *B* and *E*).

Nucleobase Stacking and Abasic Site Bypass—Superior stacking and solvation properties of adenine have been discussed as a driving force behind adenine selection opposite abasic sites (17, 29–31). The nucleotide dNITP contains a nucleobase surrogate lacking hydrogen-bonding capability but increased stacking ability in comparison with their structural congener purines. These properties build the basis for the motivation to employ the nucleotide in abasic site bypass (17, 31, 48–50). We find, in contrast to the results obtained with nucleotides containing the natural nucleobases, that binding of the nucleotide analog dNITP readily allows the enzyme to change its active site conformation in a closed, productive complex that is similar to those found for undamaged DNA substrates. The accumulation of the enzyme in a productive conformation is clearly supported by the kinetic data, which show a significant increase in incorporation efficiency of dNIMP as compared with dAMP opposite the abasic site. Furthermore, the circumstance that dNITP is processed with higher efficiency than the favored nucleotides of either *KlenTaq* wild type or *KlenTaq* mutant Y671W shows that Tyr-671 apparently lost its selection criteria because both the dNITP and the Tyr-671 residues are not compatible with the geometric constraints of the active site. Our results suggest that due to its increased stacking ability, the nucleobase surrogate imposes active site conformations that differ significantly from those induced by the natural nucleobases. Consequently, results that are obtained by usage of dNITP instead of the natural nucleotides should be interpreted with caution toward their significance in abasic site bypass by natural nucleotides. It is noteworthy that dNITP is known as a chain terminator (59, 60) as well as universal base (61) and has shown no preference for incorporation opposite one of the four natural nucleobases. Again, enforcement of aberrant enzyme and DNA conformations due to the strong stacking ability of dNITP might be the origin of the observed properties.

Taken together, the present structural study of *KlenTaq* in complex with different nucleoside triphosphates opposite an abasic site reveals that natural nucleotides are bound, due to interaction with Tyr-671 and the geometric confines of the active site, in positions that require additional conformational changes for proper alignment to facilitate the chemical step. The degree of misalignment, measured as distance of the α-phosphate to the 3′-primer terminus, parallels the order of incorporation efficiency of *KlenTaq* opposite an abasic site. These conformational changes might be accompanied by barriers of varied energy explaining the observed decline in nucleotide incorporation efficiency from A and G to T and C as well as the strong block of the abasic site lesion. The resulting pausing of DNA synthesis might allow the DNA polymerase to be replaced by repair systems that use the sister strand for error-free repair.

The human DNA polymerase θ and γ are members of the sequence family A as *KlenTaq*. Interestingly, the human DNA polymerase θ also obeys the A-rule (18), and its intrinsically error-prone abasic site bypass might contribute to somatic hypermutation of Ig genes (62). Furthermore, the role of Tyr-671 in nucleotide selection opposite an abasic site is highlighted. Tyr-671 is highly conserved in family A DNA polymerases (19, 34) and is known to be involved in the discrimination process between canonical and noncanonical base pairs (63–65). Along these lines, Leob and co-workers (63) demonstrated that Tyr-671 is essential for maintaining *Taq* DNA polymerase I activity. Mutations at that position are hardly tolerated and compromise activity with the exception of phenylalanine. Nevertheless, mutations of the homolog residue Tyr-766 of the Klenow fragment from *E. coli* DNA polymerase I to serine or alanine result in significant decrease in fidelity (64). Interestingly, mutation of the corresponding Tyr-955 in human DNA polymerase γ has been attributed to progressive external ophthalmoplegia, stressing its importance in accurate function of DNA polymerases (58, 66).

Acknowledgments—We thank the beamline staff of the Swiss Light Source (SLS) and Konstanz Research School Chemical Biology for support.

REFERENCES

1. Lindahl, T. (1993) Instability and decay of the primary structure of DNA. *Nature* **362,** 709–715
2. Loeb, L. A., and Preston, B. D. (1986) Mutagenesis by apurinic/apyrimidinic sites. *Annu. Rev. Genet.* **20,** 201–230
3. Hoeijmakers, J. H. (2001) Genome maintenance mechanisms for preventing cancer. *Nature* **411,** 366–374
4. Avkin, S., Adar, S., Blander, G., and Livneh, Z. (2002) Quantitative measurement of translesion replication in human cells: evidence for bypass of abasic sites by a replicative DNA polymerase. *Proc. Natl. Acad. Sci. U.S.A.* **99,** 3764–3769
5. Goodman, M. F., Cai, H., Bloom, L. B., and Eritja, R. (1994) Nucleotide insertion and primer extension at abasic template sites in different sequence contexts. *Ann. N.Y. Acad. Sci.* **726,** 132–142
6. Hubscher, U., Maga, G., and Spadari, S. (2002) Eukaryotic DNA polymerases. *Annu. Rev. Biochem.* **71,** 133–163
7. Pagès, V., Johnson, R. E., Prakash, L., and Prakash, S. (2008) Mutational

specificity and genetic control of replicative bypass of an abasic site in yeast. *Proc. Natl. Acad. Sci. U.S.A.* **105,** 1170–1175
8. Schaaper, R. M., Kunkel, T. A., and Loeb, L. A. (1983) Infidelity of DNA synthesis associated with bypass of apurinic sites. *Proc. Natl. Acad. Sci. U.S.A.* **80,** 487–491
9. Sagher, D., and Strauss, B. (1983) Insertion of nucleotides opposite apurinic/apyrimidinic sites in deoxyribonucleic acid during *in vitro* synthesis: uniqueness of adenine nucleotides. *Biochemistry* **22,** 4518–4526
10. Randall, S. K., Eritja, R., Kaplan, B. E., Petruska, J., and Goodman, M. F. (1987) Nucleotide insertion kinetics opposite abasic lesions in DNA. *J. Biol. Chem.* **262,** 6864–6870
11. Efrati, E., Tocco, G., Eritja, R., Wilson, S. H., and Goodman, M. F. (1997) Abasic translesion synthesis by DNA polymerase β violates the "A-rule": novel types of nucleotide incorporation by human DNA polymerase β at an abasic lesion in different sequence contexts. *J. Biol. Chem.* **272,** 2559–2569
12. Shibutani, S., Takeshita, M., and Grollman, A. P. (1997) Translesional synthesis on DNA templates containing a single abasic site: a mechanistic study of the "A-rule". *J. Biol. Chem.* **272,** 13916–13922
13. Strauss, B. S. (2002) The "A-rule" revisited: polymerases as determinants of mutational specificity. *DNA Repair* **1,** 125–135
14. Taylor, J. S. (2002) New structural and mechanistic insight into the A-rule and the instructional and non-instructional behavior of DNA photoproducts and other lesions. *Mutat. Res.* **510,** 55–70
15. Freisinger, E., Grollman, A. P., Miller, H., and Kisker, C. (2004) Lesion (in)tolerance reveals insights into DNA replication fidelity. *EMBO J.* **23,** 1494–1505
16. Hogg, M., Wallace, S. S., and Doublié, S. (2004) Crystallographic snapshots of a replicative DNA polymerase encountering an abasic site. *EMBO J.* **23,** 1483–1493
17. Reineks, E. Z., and Berdis, A. J. (2004) Evaluating the contribution of base stacking during translesion DNA replication. *Biochemistry* **43,** 393–404
18. Seki, M., Masutani, C., Yang, L. W., Schuffert, A., Iwai, S., Bahar, I., and Wood, R. D. (2004) High-efficiency bypass of DNA damage by human DNA polymerase Q. *EMBO J.* **23,** 4484–4494
19. Obeid, S., Blatter, N., Kranaster, R., Schnur, A., Diederichs, K., Welte, W., and Marx, A. (2010) Replication through an abasic DNA lesion: structural basis for adenine selectivity. *EMBO J.* **29,** 1738–1747
20. Obeid, S., Schnur, A., Gloeckner, C., Blatter, N., Welte, W., Diederichs, K., and Marx, A. (2011) Learning from directed evolution: *Thermus aquaticus* DNA polymerase mutants with translesion synthesis activity. *ChemBioChem* **12,** 1574–1580
21. Ling, H., Boudsocq, F., Woodgate, R., and Yang, W. (2004) Snapshots of replication through an abasic lesion: structural basis for base substitutions and frameshifts. *Mol. Cell* **13,** 751–762
22. Fiala, K. A., Hypes, C. D., and Suo, Z. (2007) Mechanism of abasic lesion bypass catalyzed by a Y-family DNA polymerase. *J. Biol. Chem.* **282,** 8188–8198
23. Nair, D. T., Johnson, R. E., Prakash, L., Prakash, S., and Aggarwal, A. K. (2009) DNA synthesis across an abasic lesion by human DNA polymerase ι. *Structure* **17,** 530–537
24. Choi, J. Y., Lim, S., Kim, E. J., Jo, A., and Guengerich, F. P. (2010) Translesion synthesis across abasic lesions by human B-family and Y-family DNA polymerases α, δ, η, ι, κ, and REV1. *J. Mol. Biol.* **404,** 34–44
25. Sherrer, S. M., Fiala, K. A., Fowler, J. D., Newmister, S. A., Pryor, J. M., and Suo, Z. (2011) Quantitative analysis of the efficiency and mutagenic spectra of abasic lesion bypass catalyzed by human Y-family DNA polymerases. *Nucleic Acids Res.* **39,** 609–622
26. Nair, D. T., Johnson, R. E., Prakash, L., Prakash, S., and Aggarwal, A. K. (2011) DNA synthesis across an abasic lesion by yeast REV1 DNA polymerase. *J. Mol. Biol.* **406,** 18–28
27. Yang, W., and Woodgate, R. (2007) What a difference a decade makes: insights into translesion DNA synthesis. *Proc. Natl. Acad. Sci. U.S.A.* **104,** 15591–15598
28. Zahn, K. E., Wallace, S. S., and Doublié, S. (2011) DNA polymerases provide a canon of strategies for translesion synthesis past oxidatively generated lesions. *Curr. Opin. Struct. Biol.* **21,** 358–369
29. Matray, T. J., and Kool, E. T. (1999) A specific partner for abasic damage in DNA. *Nature* **399,** 704–708
30. Hwang, H., and Taylor, J. S. (2004) Role of base stacking and sequence context in the inhibition of yeast DNA polymerase η by pyrene nucleotide. *Biochemistry* **43,** 14612–14623
31. Zahn, K. E., Belrhali, H., Wallace, S. S., and Doublié, S. (2007) Caught bending the A-rule: crystal structures of translesion DNA synthesis with a non-natural nucleotide. *Biochemistry* **46,** 10551–10561
32. Goodman, M. F. (1997) Hydrogen bonding revisited: geometric selection as a principal determinant of DNA replication fidelity. *Proc. Natl. Acad. Sci. U.S.A.* **94,** 10493–10495
33. Kool, E. T. (2002) Active site tightness and substrate fit in DNA replication. *Annu. Rev. Biochem.* **71,** 191–219
34. Delarue, M., Poch, O., Tordo, N., Moras, D., and Argos, P. (1990) An attempt to unify the structure of polymerases. *Protein Eng.* **3,** 461–467
35. Li, Y., Korolev, S., and Waksman, G. (1998) Crystal structures of open and closed forms of binary and ternary complexes of the large fragment of *Thermus aquaticus* DNA polymerase I: structural basis for nucleotide incorporation. *EMBO J.* **17,** 7514–7525
36. Di Pasquale, F., Fischer, D., Grohmann, D., Restle, T., Geyer, A., and Marx, A. (2008) Opposed steric constraints in human DNA polymerase β and *E. coli* DNA polymerase I. *J. Am. Chem. Soc.* **130,** 10748–10757
37. Kabsch, W. (2010) XDS. *Acta Crystallogr. D* **66,** 125–132
38. Kabsch, W. (2010) Integration, scaling, space-group assignment, and post-refinement. *Acta Crystallogr. D* **66,** 133–144
39. Adams, P. D., Grosse-Kunstleve, R. W., Hung, L. W., Ioerger, T. R., McCoy, A. J., Moriarty, N. W., Read, R. J., Sacchettini, J. C., Sauter, N. K., and Terwilliger, T. C. (2002) PHENIX: building new software for automated crystallographic structure determination. *Acta Crystallogr. D* **58,** 1948–1954
40. Emsley, P., and Cowtan, K. (2004) Coot: model-building tools for molecular graphics. *Acta Crystallogr. D* **60,** 2126–2132
41. DeLano, W. L. (2010) *The PyMOL Molecular Graphics System*, version 1.3r1, Schrödinger, LLC, New York
42. Li, Y., Mitaxov, V., and Waksman, G. (1999) Structure-based design of *Taq* DNA polymerases with improved properties of dideoxynucleotide incorporation. *Proc. Natl. Acad. Sci. U.S.A.* **96,** 9491–9496
43. Li, Y., and Waksman, G. (2001) Crystal structures of a ddATP-, ddTTP-, ddCTP, and ddGTP- trapped ternary complex of Klentaq1: insights into nucleotide incorporation and selectivity. *Protein Sci.* **10,** 1225–1233
44. Obeid, S., Baccaro, A., Welte, W., Diederichs, K., and Marx, A. (2010) Structural basis for the synthesis of nucleobase modified DNA by *Thermus aquaticus* DNA polymerase. *Proc. Natl. Acad. Sci. U.S.A.* **107,** 21327–21331
45. Betz, K., Streckenbach, F., Schnur, A., Exner, T., Welte, W., Diederichs, K., and Marx, A. (2010) Structures of DNA polymerases caught processing size-augmented nucleotide probes. *Angew. Chem., Int. Ed. Engl.* **49,** 5181–5184
46. Korolev, S., Nayal, M., Barnes, W. M., Di Cera, E., and Waksman, G. (1995) Crystal structure of the large fragment of *Thermus aquaticus* DNA polymerase I at 2.5-Å resolution: structural basis for thermostability. *Proc. Natl. Acad. Sci. U.S.A.* **92,** 9264–9268
47. Wintjens, R., Liévin, J., Rooman, M., and Buisine, E. (2000) Contribution of cation-π interactions to the stability of protein-DNA complexes. *J. Mol. Biol.* **302,** 395–410
48. Vineyard, D., Zhang, X., Donnelly, A., Lee, I., and Berdis, A. J. (2007) Optimization of non-natural nucleotides for selective incorporation opposite damaged DNA. *Org. Biomol. Chem.* **5,** 3623–3630
49. Sheriff, A., Motea, E., Lee, I., and Berdis, A. J. (2008) Mechanism and dynamics of translesion DNA synthesis catalyzed by the *Escherichia coli* Klenow fragment. *Biochemistry* **47,** 8527–8537
50. Motea, E. A., Lee, I., and Berdis, A. J. (2011) Quantifying the energetic contributions of desolvation and π-electron density during translesion DNA synthesis. *Nucleic Acids Res.* **39,** 1623–1637
51. Joyce, C. M., and Benkovic, S. J. (2004) DNA polymerase fidelity: kinetics, structure, and checkpoints. *Biochemistry* **43,** 14317–14324
52. Johnson, K. A. (2010) The kinetic and chemical mechanism of high-fidelity DNA polymerases. *Biochim. Biophys. Acta* **1804,** 1041–1048
53. Joyce, C. M. (2010) Techniques used to study the DNA polymerase reac-

tion pathway. *Biochim. Biophys. Acta* **1804,** 1032–1040
54. Wu, E. Y., and Beese, L. S. (2011) The structure of a high-fidelity DNA polymerase bound to a mismatched nucleotide reveals an "ajar" intermediate conformation in the nucleotide selection mechanism. *J. Biol. Chem.* **286,** 19758–19767
55. Santoso, Y., Joyce, C. M., Potapova, O., Le Reste, L., Hohlbein, J., Torella, J. P., Grindley, N. D., and Kapanidis, A. N. (2010) Conformational transitions in DNA polymerase I revealed by single-molecule FRET. *Proc. Natl. Acad. Sci. U.S.A.* **107,** 715–720
56. Florián, J., Goodman, M. F., and Warshel, A. (2005) Computer simulations of protein functions: searching for the molecular origin of the replication fidelity of DNA polymerases. *Proc. Natl. Acad. Sci. U.S.A.* **102,** 6819–6824
57. Batra, V. K., Beard, W. A., Shock, D. D., Pedersen, L. C., and Wilson, S. H. (2008) Structures of DNA polymerase β with active site mismatches suggest a transient abasic site intermediate during misincorporation. *Mol. Cell* **30,** 315–324
58. Graziewicz, M. A., Longley, M. J., Bienstock, R. J., Zeviani, M., and Copeland, W. C. (2004) Structure-function defects of human mitochondrial DNA polymerase in autosomal dominant progressive external ophthalmoplegia. *Nat. Struct. Mol. Biol.* **11,** 770–776
59. Smith, C. L., Simmonds, A. C., Felix, I. R., Hamilton, A. L., Kumar, S., Nampalli, S., Loakes, D., Hill, F., and Brown, D. M. (1998) DNA polymerase incorporation of universal base triphosphates. *Nucleosides Nucleotides* **17,** 541–554
60. Loakes, D. (2001) Survey and summary: the applications of universal DNA base analogues. *Nucleic Acids Res.* **29,** 2437–2447
61. Loakes, D., and Brown, D. M. (1994) 5-Nitroindole as a universal base analogue. *Nucleic Acids Res.* **22,** 4039–4043
62. Masuda, K., Ouchida, R., Hikida, M., and Kurosaki, T. (2007) DNA polymerases η and θ function in the same genetic pathway to generate mutations at A/T during somatic hypermutation of Ig genes. *J. Biol. Chem.* **282,** 17387–17394
63. Suzuki, M., Baskin, D., Hood, L., and Loeb, L. A. (1996) Random mutagenesis of *Thermus aquaticus* DNA polymerase I: concordance of immutable sites *in vivo* with the crystal structure. *Proc. Natl. Acad. Sci. U.S.A.* **93,** 9670–9675
64. Bell, J. B., Eckert, K. A., Joyce, C. M., and Kunkel, T. A. (1997) Base miscoding and strand misalignment errors by mutator Klenow polymerases with amino acid substitutions at tyrosine 766 in the O helix of the fingers subdomain. *J. Biol. Chem.* **272,** 7345–7351
65. Minnick, D. T., Bebenek, K., Osheroff, W. P., Turner, R. M., Jr., Astatke, M., Liu, L., Kunkel, T. A., and Joyce, C. M. (1999) Side chains that influence fidelity at the polymerase active site of *Escherichia coli* DNA polymerase I (Klenow fragment). *J. Biol. Chem.* **274,** 3067–3075
66. Copeland, W. C., Ponamarev, M. V., Nguyen, D., Kunkel, T. A., and Longley, M. J. (2003) Mutations in DNA polymerase γ cause error-prone DNA synthesis in human mitochondrial disorders. *Acta Biochim. Pol.* **50,** 155–167